Blue emission and twin structure of p-type copper iodide thin films

O. Madkhali, Maud Jullien, Alaa E. Giba, J. Ghanbaja, S. Mathieu, C. Gendarme, Sylvie Migot, Y. Alajlani, N. Can, F. Alnjiman, et al.

Version of Record: https://www.sciencedirect.com/science/article/pii/S2468023021005770
Manuscript_d4b7574bb92427043eb4893d352aaa46

Blue emission and twin structure of p-type copper iodide thin films

O. Madkhali [1,2], M. Jullien [1], Alaa E. Giba [1,3], J. Ghanbaja [1], S. Mathieu [1], C. Gendarme [1], S. Migot [1], Y. Alajlani [2], N. Can [2], F. Alnjiman [1,4], D. Horwat [1], A. Redjaimia[1], J.F. Pierson [1,*]

[1] Institut Jean Lamour (UMR CNRS 7198), Université de Lorraine, Nancy, France

[2] Department of Physics at College of Science, Jazan University at Jazan, Saudi Arabia

[3] National Institute of Laser Enhanced Sciences, Cairo University, Giza 12613, Egypt

[4] Department of Physics and astronomy at College of Science, King Saud University at Riyadh, Riyadh, Saudi Arabia

* Corresponding author: jean-francois.pierson@univ-lorraine.fr

Abstract

Copper iodide is an attractive p-type transparent material suitable for optoelectronic applications. This work reports on the synthesis of copper iodide (CuI) by iodination of sputtered Cu films previously deposited on glass and silicon substrates. The crystalline phase and surface morphology were studied by X-ray diffraction (XRD) and scanning electron microscopy (SEM), respectively. The prepared CuI films crystallize in the zinc blende structure (γ-phase) at different amounts of iodine and exhibit preferential orientation along the <111> direction. Moreover, detailed investigation of the microstructure via high-resolution transmission electron microscopy (HR-TEM) revealed the presence and details of alternating twin crystallographic domains between adjacent grains. The electrical properties of the CuI films were characterized by Hall effect measurements and revealed a p-type carrier behavior for all films. The electrical behavior was discussed and attributed to the change in intrinsic point defects. In addition, the electronic bandgap and luminescence properties were investigated using optical transmission and photoluminescence (PL). The CuI films showed a wide band gap (about 3.05 eV) with an average transmittance of about (66 %) in the visible region. Moreover, the PL showed a blue emission ranging from 400 to 440 nm originating from the excitonic recombination and radiative point defects.

Keywords: Copper iodide, Semiconductor, Twinning, Optoelectronic applications

1. Introduction

Copper iodide (CuI) has attracted much attention during the last century[1]. Due to its controllable crystal structure and the excellent optical and electrical properties, it led to recent and promising applications in the optoelectronic field[2–4]. CuI crystallises in three structures: α, β and γ depending on the growth temperature [1,5,6]. α, β and γ adopt rocksalt, wurtzite and zinc blende structures at temperature higher than 673 K, between 643 - 673 K and lower than 643 K, respectively. These three phases crystallise in $Fm\bar{3}m$, P3m1 and $F\bar{4}3m$ space groups. The reported values of lattice parameters are: $a_\alpha = 0.616866\,nm$, $a_\beta = 0.4279\,nm$, $c_\beta = 0.7168\,nm$ and $a_\gamma = 0.605844\,nm$. This diversity in crystal structure makes CuI adaptable to different heterostructure regimes with multiple materials[7]. For example, the low lattice mismatch between the zinc blende structure of copper halides with Si substrate makes it a promising candidate for epitaxial growth[8]. This is an advantage over the well-known commercial wurtzite semiconductors: GaN and ZnO, also used in optoelectronic applications [9,10]. This also indicates the compatibility of CuI with Si technology. Unlike the wurtzite structure, zinc blende reduces the internal piezoelectric property, which improves performance of the optoelectronic devices. In addition, the ease of synthesis and high performance of CuI at low and room temperature favor its competition with other transparent conductive materials (TCMs)[11].

From the optoelectronic point of view, CuI is considered as wide (about 3.1 eV)[1,11–15] and direct bandgap material with high exciton binding energy of about 62 meV[1,16]. This wide bandgap and high exciton binding energy are promising features for UV-blue emitting devices with high quantum efficiency[17] with possible operation at room temperature. Moreover, it exhibits intrinsic conductivity of p-type charge carriers. It is worth mentioning that the intrinsic optical and electrical properties of CuI are based on point defect chemistry. Thus, the p-type conductivity of CuI is due to the dominance of Cu-vacancy defects because of their low formation energy[1,18]. In contrast, formation of I-defects leads to the generation of a donor level which can compensate for the acceptors generated by Cu defects. Therefore, the control of defect chemistry in CuI is of great importance. This is considered as a practical way to tune and adjust the electrical response of the CuI. In this line, photoluminescence (PL) is a non-destructive and efficient tool that helps to identify and understand the role of such defects. Thanks to the inclusion of these point defects in

the radiative recombinations, PL measurements not only lead to identification of the nature of the defects, but also provide information about the emission colour properties of the material.

Various techniques such as thermal evaporation[18], sputtering[19], mister atomizer[20], ionization[21], sputtering with excess iodine[22], and pulsed laser deposition[23] have been used to prepare CuI thin films. However, depending on the synthesis method, CuI films exhibit a wide range of properties, such as in figure of merit (FOM), which ranges from 350 [21] to 17000 $M\Omega^{-1}$ [22]. Among these thin film growth methods, thermal evaporation and sputtering are simpler and provide acceptable results compared to alternative methods. Compared to all these techniques, a two step process including the deposition of a copper thin film and its iodination is simpler. Indeed such a two step process avoids to introduce gaseous iodine into vacuum chambers that may contaminate the deposition chamber walls for the elaboration other kind of coatings (metals, nitrides…). Such a process also allows better control in terms of thickness, process duration and iodine addition amount. The maximum values of hole mobility of CuI films reported in the literature were 25 $cm^2 V^{-1} s^{-1}$ for polycrystalline films[24] and pulsed laser deposition[25]. Even higher hole mobilities are possible, such as 43.9 $cm^2 V^{-1} s^{-1}$ for the bulk material.[13] Although CuI thin films have been widely studied during the last decade, surprisingly the literature does not present a detailed characterization of such films using transmission electron microscopy (TEM).

As discussed above, it is clear that deep structural, optical, and electrical studies are of great importance to better understand the functional properties of CuI. In this work, high resolution TEM was used to explore in details the structure of the prepared films at the nanoscale. Electrical characterizations were also performed to investigate the electrical conductivity and mobility of the films. PL spectrocopy was used to characterize the luminescence contributions of the point defects.

2. Experimental procedure

Metallic copper thin films were deposited at room temperature by magnetron sputtering of a metallic copper target in the presence of an argon plasma. Copper thin films were deposited on glass and (100) single crystal silicon substrates (2 x 2 cm^2) by magnetron sputtering of a 5 cm diameter and 3 mm thick copper target (purity > 99.99 %). The argon flow rate was set at 30 standard cubic centimeters per minute (sccm). Prior to placement in the deposition chamber, the substrates were ultrasonically cleaned with ethanol during approximately 3 minutes for each

sample. Drying was performed with a dust-free air flow. Prior to deposition, an etching step was performed using a radiofrequency (RF) plasma (13.56 MHz) to clean the surface of the substrates. During the growth process, thin films were deposited at a total sputtering pressure of 0.5 Pa. The current applied to the target was fixed at 0.3 A using an Advanced Energy Pinnacle+ pulsed-DC power supply with a frequency of 50 kHz and an off-time of 4 µs. The distance between the substrate and the target was fixed at 5.5 cm. The thickness of the deposited copper films was set to 50 nm.

After the Cu deposition, the samples were removed from the vacuum chamber and were placed into another reactor. The Cu films, placed in a Pyrex® vessel, were heated from room temperature to 75 °C. When the temperature was fixed to 75 °C, a certain amount of solid iodine was introduced into the reaction chamber. Due to its high vapor pressure, the solid iodine sublimates and forms the useful vapor for the iodination reaction [26,27]. Thus, the atmosphere of the reaction chamber was a mixture of air and iodine vapor. Since the reaction took place at low temperature (75 °C) the kinetic of the copper oxidation reaction was too low to induce the formation of a copper oxide layer and only copper iodide was formed. After 60 minutes duration, the process was stopped by water cooling of the reaction chamber.

The film composition was measured using a JEOL 8530-F electron probe microanalyzer (EPMA). Quantitative measurements were performed at 20 kV and 50 nA, using Cu and RbI standards. The film structure was characterized by θ–2θ X-ray diffraction (XRD) using a Bruker D8 Advance diffractometer with copper $K_{\alpha 1}$ radiation (λ = 0.15406 nm). Morphology of the CuI layer was evaluated by scanning electron microscopy (SEM) at 3 kV using a field emission gun ZEISS Gemini SEM 500 microscope. Transmission electron microscopy (TEM) was performed using a JEOL ARM 200-Cold FEG (point resolution 0.19 nm). To avoid CuI decomposition under the electron beam, the sample holder was cooled with liquid nitrogen. The cross-sectional TEM sample was prepared using a focused ion beam (FIB)-SEM dual beam system (FEI Helios Nanolab 600i). Optical properties were characterized by transmittance measurements in the 300-800 nm range using a Varian Cary 5000 spectrophotometer. The photoluminescence (PL) measurements were performed using a spectrofluorometer (Fluorolog-Horiba). A xenon arc lamp source (320 nm) was used, and the PL emission was analyzed with a detection system equipped with 150 grooves/mm gratings and a cooled silicon-based CCD camera. The resistivity, carrier density and

mobility were derived from Hall measurements at room temperature in van der Pauw geometry (Ecopia, HMS-5000).

3. Results and discussion

3.1.Structure and composition of CuI films

The X-ray diffractogram of the deposited copper film is shown in Figure 1a. The (111) and (200) crystallographic planes of this fcc material can be clearly seen and the metallic Cu film have been grown with a preferred orientation along the [111] direction. The X-ray diffractograms of iodinated films obtained with different amounts of iodine on silicon substrate are shown in Figure 1b. Regardless the amount of I_2, the iodinated films are highly crystallized. The same conclusion can be drawn when glass substrates (not shown here) are used. The position of the diffraction peaks fits well with the γ-CuI structure in agreement with the phase diagram of this material. The X-ray diffractogram of CuI films exhibits peaks corresponding to the (111), (200), (220) and (311) diffraction planes of the zinc blende structure at about 25, 30, 42 and 50°, respectively [1,12,28–34]. Since no metallic copper diffraction peak is detectable after the iodination step, the 50-nm thick sputtered Cu films are completely iodinated after the reaction at 75 °C for 60 minutes. Since the intensity of the (111) diffraction is very high compared to the other peaks, the CuI films show a preferential orientation along the [111] direction. This preferred orientation is similar to that observed on the metallic Cu film. However the relative intensity of the (200) planes is lower for the copper iodide film suggesting that the preferred orientation of the CuI film may originate both from the preferred orientation of the metallic Cu film and from the peculiarities of iodine diffusion. The lattice parameter derived from the peak position is $a = 0.6048 \pm 0.0073$ nm. This experimental value is close to the theoretical one ($a = 0.6054$ nm). The average crystallite size was determined using Scherrer's formula. For the different values of iodine mass, the coherence length is ranging between 53 and 67 nm ± 7 nm, while for the deposited copper the coherence length is about 35 ± 4 nm. This twofold size increase has to be compared with that expected from the volume expansion is 4.7 (see section 3.2.). Such difference may come from the introduction of defects into the CuI grain that limit the coherence length.

The composition of the copper iodide film was measured by electron probe microanalysis. The iodine mass does not have a strong influence on the film composition and the film prepared with

0.15 g I_2 has the following composition: 52.8 at. % for I and 47.2 at. % for Cu. From these values, the atomic I/Cu ratio is about 1.12, suggesting an iodine over stoichiometry and then the occurrence of copper vacancies. Although the increase of the iodine amount does not influence the CuI film composition, an increase of the Cu (111) diffraction peak was noticed. These results may suggest that the increase of the iodine amount favors the CuI film crystallinity.

3.2. Microstructure of γ-CuI thin films

The cross section of a CuI layer is shown in Figure 2a. Compared to the deposited Cu, this SEM image clearly shows that the film surface is no longer smooth. Moreover, no porosity can be seen on this fracture image. The thickness estimated from this image is about 300 nm. As-deposited copper films have a thickness of 50 nm. Since the ratio between the molar volume of CuI (33.39 $cm^3\ mol^{-1}$) and that of copper (7.11 $cm^3\ mol^{-1}$) is 4.7, the thickness measured by SEM (300 nm) is close to that expected (235 nm). This result also confirms that the iodination reaction is complete. The surface morphology of the films shows that they are composed of flat and contiguous equiaxed crystals (Figure 2b). Some porosities, which could not be detected in the cross section, can be observed on the surface image. The film morphology is independent of the nature of the substrate. A magnification of the surface of a film obtained on a glass substrate is shown in Figure 2c. Again, large grains and porosities can be observed. Such porosities may explain the difference between the expected and measured film thickness. The average grain size derived from Figure 2c and estimated using the ImageJ software is 260 nm. This value is very high compared to the value estimated by the Scherrer formula, and we will elaborate in the following on the origin of this difference. An interesting point is the appearance of some straight lines on the copper iodide grains. Such behavior has already been observed in the literature[1,35] but there is no clear description of the meaning of such lines. In order to obtain relevant information about these lines, the films were characterized by transmission electron microscopy.

Although copper iodide thin films have been widely studied in the literature, there are few works that provide a detailed characterization of CuI by TEM[36]. This may be due to the fact that CuI film reduce into to copper under the electron beam. To avoid such decomposition, TEM characterization should be carried out at the temperature of liquid nitrogen. Under this condition,

the decomposition of CuI is inhibited. Figure 3a shows a TEM cross-sectional view of a CuI thin film. The film thickness is consistent with that previously measured using SEM cross section. Interestingly, no porosities can be seen in the analysed film cross section, indicating that density of such porosities is rather low . The CuI film contains large grains with a length of several hundred nanometers on the film surface. Electron diffraction confirms that the film crystallizes in the γ-CuI structure with a lattice parameter a = 0.615 nm (Figure 3b).

In Figure 2c, straight lines can be seen on the grain surface. Such lines can also be seen on the TEM cross-section (Figure 3a). These lines, which pass through the entire layer thickness and reach the film surface are suspected of being to twins. Detailed TEM and electron diffraction analysis revealed that these very thin lines are the traces of the twinning planes separating two contiguous variants. The latter are twin-related as indicated by the composite selected area diffraction pattern (SAED), recorded along $[10\bar{1}]_I//[\bar{1}01]_{II}$. Trace analysis supported by the bright field TEM micrograph (Figure 3a) and the corresponding diffraction patterns (Figure 3b and 3c) indicate that the twinning plane is (111). This twinning plane is expected as the γ-CuI crystallises in the FCC structure. The twinning (111) planes can be also understood according to Yang et al., where the Wulff shapes of CuI fcc crystals had been simulated and demonstrated for reactively sputtered CuI films [37] .

One can notice, on the diffraction pattern, diffusion lines running parallel to (111) direction and crossing the (002) and $(11\bar{1})$ reflections, belonging to type I and type II, respectively. This diffusion lines are perpendicular to the trace of the (111) twinning plane. This situation is further a practical way to identify the (111) twinning plane. The bright (Fig. 3a) and dark field (Figure 4a, b, and c) images highlight the twinning plane separating the alternating twin-related variants following the sequence: I, II, I.

Figure 4 shows TEM dark fields images, showing twinned variants of a thin CuI film deposited on a silicon substrate. TEM dark field images taken with $\vec{g}_I = (002)$ and $\vec{g}_{II} = (11\bar{1})$, respectively, highlight prominence of two twin-related variants, labelled I and II (Figures 4a and 4b). The twin variant of type II is bordered on its most elongated parallel sides by two twin-variants of the type I (Figure 4c).

STEM analyses were performed on the same area to localize iodine atoms in the thin film (Fig. 5). Along the analytical line, the iodine and copper concentrations are almost constant. The inset fast Fourier transform (FFT) and the corresponding high resolution images indicate planes with their *d*-spacings of 0.35 nm and 0.31 nm, corresponding to the d_{111} and d_{200} of the γ-CuI phase, respectively.

3.3. Optical transmission and absorption

The transmittance and absorption coefficient (α) of the γ-CuI film synthesized with different amounts of iodine are shown in Figure 6a. As can be seen from this figure, a mean transmittance of 66 % is obtained in the 400-800 nm range when a mass of 0.5 g of iodine was used. Such transmittance value is close to the reported values[19,22]. It can be observed that the sample synthesized with 0.20 g of I2 shows the lowest transmission value while the sample synthesized with 0.5 g of I2 exhibit the highest one. This change in the transmission value can be correlated and understood from the crystallinity point of view. Sample with the lowest transmittance is characterized by the smaller crystallites size, approx. 50 nm, while the sample with the highest transmittance exhibits a coherence length of 65 nm. Hence, smaller crystallites size means high density of the grain boundaries, which lead to scattering of more light and eventually low optical transmission is obtained. A strong absorption is observed at a wavelength close to 400 nm, which corresponds to the band gap of the film. This parameter was determined by the Tauc method, taking into account that γ-CuI is a direct semiconductor. Under our synthesis conditions, the optical band gap is estimated around 3.05 eV, which is agreement with literature [1,11–13,15,36,38]and the theoretical value of 3.203 eV[14] obtained using the PBE0 calculation method[39]. Figure 6.b shows the evolution of the absorption coefficient as a function of wavelength. The shape of this curve is typical of γ-CuI , showing two maxima : one at 337 nm (3.68 eV) and the second one at 407 nm (3.04 eV). This behaviour is attributed to the onset of the optical band gap of CuI. It has been reported that the origin of these two peaks are the direct optical transitions at the Γ point, called $Z_{1,2}$ and Z_3, respectively [40].

Indeed, the first peak $(Z_{1,2})$ consists essentially of a doublet structure corresponding to heavy-hole (HH) and light-hole (LH)excitons, as reported in [40]. On the other hand, the later peak (Z_3) is assigned to the split-off-hole exciton. It is worth noting that the splitting of energy

between the HH and LH is evident at low temperature due to the localization of charge carrier motion. However, careful focus on the $Z_{1,2}$ peak in the present study reveals an asymmetry of the peak maximum that can be attributed to the low splitting energy between the HH and LH at room temperature. This is consistent with the view of Kim *et al.* [40] who showed that this splitting energy decreases with the increase in the temperature.

3.4. Electrical properties

The conductivity, charge carrier density and mobility of CuI films are presented in Table 1. They were derived from Hall effect measurements using van der Pauw geometry. Regardless the amount of iodine, the films show p-type behavior. At room temperature, the conductivity (σ) of the CuI thin films ranges from 19.6 to 47.4 S cm^{-1}. Despite the presence of defects deduced from XRD analyses and observed by TEM characterization, the electrical conductivity of CuI films is higher than the reported values [11,20,21]. An optimum of the film conductivity is observed for 0.15 g of iodine. The obtained value of conductivity (47.4 S cm^{-1}) is very high compared to other p-type materials such as Cu_2O [41] or $CuCrO_2$ [42]. This result clearly confirms that CuI is a suitable material for p-type transparent conductive thin films. Therefore, the reason for p-type conductivity is due to the occurrence of copper vacancies, resulting from their low formation energy compared with other copper iodide defects [1,14,22,43,44]. The mobility of holes in CuI thin films prepared at room temperature is higher than that of spiro-MeOTAD with 4×10^{-5} cm^2 V^{-1} s^{-1} [45] and that of CuSCN (0.1 cm^2 V^{-1} s^{-1}) [46]. Therefore, CuI thin films can serve as a strong hole transport layer for perovskite solar cells [47]. Recently, Chang et al. [22] reported an impressive conductivity of 283 S cm^{-1} for CuI thin films prepared by reactive sputtering in the presence of excess iodine. The hole density (p) ranges from 1.4×10^{18} to 4.3×10^{19} cm^{-3}.

The figure of merit (FOM) is defined as the ratio of the electrical conductivity to the absorption coefficient in the visible range. FOM is an important parameter that quantitatively describes the performance of transparent conductive thin films. The FOM of CuI thin films prepared with different amounts of iodine is shown in Table 2 and compared with the results obtained by other techniques. The high value of FOM describes good performance of transparent conductive thin films. For transparent conductive materials, there is evidence in the literature that the figure of

merit (FOM) can be used to compare the properties of the films. Within the iodine mass tested in the present study, the FOM ranges from 1000 to 1425 $M\Omega^{-1}$ (Figure 7).

3.5.Photoluminescence

Photoluminescence (PL) is a powerful technique that provides information about the optical behavior of the material under study, while the defect chemistry of γ-CuI plays an important role in its functionality [18,28,48]. Figure 8a shows the PL spectra of the prepared samples. The PL spectra of all samples have similar spectral features. It consists of two main bands around 413 nm (blue region) and 726 nm (red region). Moreover, the fine structure of the fundamental band in the blue region shows maximum at 413 nm (3 eV) and shoulder at slightly lower energy of 418 nm (2.96 eV). This shoulder became significant at I_2-excess conditions (Figure 8b). Therefore, three PL spectral features can be considered: PL1, PL2 and PL3 at 413 nm (3 eV), 418 nm (2.96 eV) and 726 nm (1.7 eV), respectively. Similar PL peaks were reported by Satoshi Koyasu *et al*. [49] and Guochen Lin *et al.* [35] for CuI material. They attributed the origin of the PL1 peak to the electronic transition from the conduction band to the valence band, while the other peaks, PL2 and PL3, are attributed to different defect-related transitions. Tracing the behavior of these defect-related PL peaks reveals a significant contribution of the PL2 peak under I_2-excess conditions, in contrast to the PL3 peak, which becomes more evident under I_2-deficient conditions. This is in agreement with the work mentioned above. This also confirms the origin of PL2 and PL3 to Cu-vacancy and I-vacancy related transitions, respectively. In other words, the very small energy difference between PL1 and PL2 indicates that Cu-vacancy forms a shallow acceptor level. This probably indicates the favorable conditions to increase the p-type conductivity. In contrast, the I-vacancy produces deep donor level. Thus, PL2 and PL3 can be assigned to the transition from conduction band to Cu vacancies and from I vacancies to valence band, respectively. As discussed above one can see the important role of the defect chemistry in CuI which, in turn, modifies its electronic structure. However, further optical studies on the samples of this study are required to understand and control the role of these defects, leading to the desired applications.

Furthermore, CuI shows strong blue emission (inset in Figure 9), which can be exploited in various lightening applications. Moreover, the intrinsic p-type conductivity property opens the door to use CuI as a promising alternative to GaN-based light emitting devices. This may be an interesting approach, especially given the current technical difficulties in fabricating highly doped p-type GaN layers.

In this regard, the chromaticity diagram is used to verify the quality of the emission colors of the phosphor as well as to show its color coordinates in relation to the coordinates of the white light zone. The coordinates of the CIE chromaticity diagram corresponding to the four samples (Figure 9) verifies their coordinates lies in the blue region with slight shifts depending on the amount of I_2. Therefore, the CuI phosphor can be used as a blue light supplier in a white light generation system. In line with this, Taehwan Jun *et al.*[50] recently reported the generation of white light emission within the Cs-Cu-I system.

Conclusion

In this work, thin CuI films were fabricated to study the structure, microstructure, and functional properties using XRD, SEM, TEM, PL, UV-visible and Hall effect techniques. We obtained copper iodide films showing a strong preferential orientation in the [111] direction. The surface morphology of the films shows that they are composed of flat disoriented grains. The crystallographic twin domains in the CuI grains were analyzed by selected area electron diffraction (SAED), revealing the twin geometry. We synthesized a transparent conductive semiconductor with unique optoelectronic properties, including wide band gap of 3.05 eV. As a result, an average transmittance of 66 % in the visible region was achieved. The photoluminescence (PL) properties of these samples were then carefully evaluated. Consequently, three PL spectral features were obtained: PL1, PL2, and PL3 at 413 nm (3 eV), 418 nm (2.96 eV), and 726 nm (1.7 eV), respectively. CuI thin films were found to host blue light emission under 320 nm excitation. Using 0.2 g I_2, the as-prepared CuI film had an electrical conductivity of 30.8 S cm^{-1} and a mobility of 35.6 cm^2 V^{-1} s^{-1}. These results clearly indicate that γ-CuI is very promising as a transparent semiconductor. Therefore, transparent p-type CuI-based semiconductors are expected to stimulate the development of transparent electronics.

Acknowledgments

O. Madkhali expresses his sincere gratitude for the support provided by the Jazan University and the Saudi Arabia Embassy in France for the PhD scholarship. The CPER MatDS project and the CC X-gamma of IJL are acknowledged for their financial and technical support, respectively.

References

[1] M. Grundmann, F.-L. Schein, M. Lorenz, T. Böntgen, J. Lenzner, H. von Wenckstern, Cuprous iodide: A p-type transparent semiconductor, history, and novel applications: Cuprous iodide, Phys. Status Solidi A. (2013) n/a-n/a. https://doi.org/10.1002/pssa.201329349.

[2] Z. Guo, J. Li, R. Pan, J. Cheng, R. Chen, T. He, All-inorganic copper(I)-based ternary metal halides: promising materials toward optoelectronics, Nanoscale. 12 (2020) 15560–15576. https://doi.org/10.1039/D0NR04220J.

[3] Á. Balog, G.F. Samu, P.V. Kamat, C. Janáky, Optoelectronic Properties of CuI Photoelectrodes, J. Phys. Chem. Lett. 10 (2019) 259–264. https://doi.org/10.1021/acs.jpclett.8b03242.

[4] P. Stakhira, V. Cherpak, D. Volynyuk, F. Ivastchyshyn, Z. Hotra, V. Tataryn, G. Luka, Characteristics of organic light emitting diodes with copper iodide as injection layer, Thin Solid Films. 518 (2010) 7016–7018. https://doi.org/10.1016/j.tsf.2010.06.051.

[5] S. Miyake, S. Hoshino, T. Takenaka, On the Phase Transition in Cuprous Iodide, J. Phys. Soc. Jpn. 7 (1952) 19–24. https://doi.org/10.1143/JPSJ.7.19.

[6] W. BÜHRER, W. HÄLG, CRYSTAL STRUCTURE OF HIGH-TEMPERATURE CUPROUS IODIDE AND CUPROUS BROMIDE, in: R.D. ARMSTRONG (Ed.), Int. Symp. Solid Ion. Ion.-Electron. Conduct., Pergamon, 1977: pp. 701–704. https://doi.org/10.1016/B978-0-08-021592-1.50010-6.

[7] K. Yao, P. Chen, Z. Zhang, J. Li, R. Ai, H. Ma, B. Zhao, G. Sun, R. Wu, X. Tang, B. Li, J. Hu, X. Duan, X. Duan, Synthesis of ultrathin two-dimensional nanosheets and van der Waals heterostructures from non-layered γ-CuI, Npj 2D Mater. Appl. 2 (2018) 1–7. https://doi.org/10.1038/s41699-018-0058-2.

[8] L. O'Reilly, O.F. Lucas, P.J. McNally, A. Reader, G. Natarajan, S. Daniels, D.C. Cameron, A. Mitra, M. Martinez-Rosas, A.L. Bradley, Room-temperature ultraviolet luminescence from γ-CuCl grown on near lattice-matched silicon, J. Appl. Phys. 98 (2005) 113512. https://doi.org/10.1063/1.2138799.

[9] A. K., Z. Lin, D. L., N. K., T. Manzur, A.F.M. Anwar, ZnO Nanostructures for Optoelectronic Applications, in: O. Sergiyenko (Ed.), Optoelectron. Devices Prop., InTech, 2011. https://doi.org/10.5772/16202.

[10] A. Janotti, C.G.V. de Walle, Fundamentals of zinc oxide as a semiconductor, Rep. Prog. Phys. 72 (2009) 126501. https://doi.org/10.1088/0034-4885/72/12/126501.

[11] N. Yamada, R. Ino, Y. Ninomiya, Truly Transparent p-Type γ-CuI Thin Films with High Hole Mobility, Chem. Mater. 28 (2016) 4971–4981. https://doi.org/10.1021/acs.chemmater.6b01358.

[12] B.M. Morais Faustino, D. Gomes, J. Faria, T. Juntunen, G. Gaspar, C. Bianchi, A. Almeida, A. Marques, I. Tittonen, I. Ferreira, CuI p-type thin films for highly transparent thermoelectric p-n modules, Sci. Rep. 8 (2018). https://doi.org/10.1038/s41598-018-25106-3.

[13] D. Chen, Y. Wang, Z. Lin, J. Huang, X. Chen, D. Pan, F. Huang, Growth Strategy and Physical Properties of the High Mobility P-Type CuI Crystal, Cryst. Growth Des. 10 (2010) 2057–2060. https://doi.org/10.1021/cg100270d.

[14] J. Wang, J. Li, S.-S. Li, Native *p* -type transparent conductive CuI via intrinsic defects, J. Appl. Phys. 110 (2011) 054907. https://doi.org/10.1063/1.3633220.

[15] C. Yang, D. Souchay, M. Kneiß, M. Bogner, H.M. Wei, M. Lorenz, O. Oeckler, G. Benstetter, Y.Q. Fu, M. Grundmann, Transparent flexible thermoelectric material based on non-toxic earth-abundant p-type copper iodide thin film, Nat. Commun. 8 (2017). https://doi.org/10.1038/ncomms16076.

[16] C. Yang, M. Kneiß, F.-L. Schein, M. Lorenz, M. Grundmann, Room-temperature Domain-epitaxy of Copper Iodide Thin Films for Transparent CuI/ZnO Heterojunctions with High Rectification Ratios Larger than 109, Sci. Rep. 6 (2016). https://doi.org/10.1038/srep21937.

[17] B. Zhao, L. Chen, W. Liu, L. Wu, Z. Lu, W. Cao, High efficiency blue light-emitting devices based on quantum dots with core-shell structure design and surface modification, RSC Adv. 11 (2021) 14047–14052. https://doi.org/10.1039/D0RA10173G.
[18] D.K. Kaushik, M. Selvaraj, S. Ramu, A. Subrahmanyam, Thermal evaporated Copper Iodide (CuI) thin films: A note on the disorder evaluated through the temperature dependent electrical properties, Sol. Energy Mater. Sol. Cells. 165 (2017) 52–58. https://doi.org/10.1016/j.solmat.2017.02.030.
[19] T. Tanaka, K. Kawabata, M. Hirose, Transparent, conductive CuI films prepared by rf-dc coupled magnetron sputtering, Thin Solid Films. 281–282 (1996) 179–181. https://doi.org/10.1016/0040-6090(96)08607-5.
[20] M.N. Amalina, Y. Azilawati, N.A. Rasheid, M. Rusop, The Properties of Copper (I) Iodide (CuI) Thin Films Prepared by Mister Atomizer at Different Doping Concentration, Procedia Eng. 56 (2013) 731–736. https://doi.org/10.1016/j.proeng.2013.03.186.
[21] F.-L. Schein, H. von Wenckstern, M. Grundmann, Transparent *p* -CuI/ *n* -ZnO heterojunction diodes, Appl. Phys. Lett. 102 (2013) 092109. https://doi.org/10.1063/1.4794532.
[22] C. Yang, M. Kneiβ, M. Lorenz, M. Grundmann, Room-temperature synthesized copper iodide thin film as degenerate p-type transparent conductor with a boosted figure of merit, Proc. Natl. Acad. Sci. 113 (2016) 12929–12933. https://doi.org/10.1073/pnas.1613643113.
[23] P.M. Sirimanne, M. Rusop, T. Shirata, T. Soga, T. Jimbo, Characterization of transparent conducting CuI thin films prepared by pulse laser deposition technique, Chem. Phys. Lett. 366 (2002) 485–489. https://doi.org/10.1016/S0009-2614(02)01590-7.
[24] N. Yamada, Y. Kondo, R. Ino, Low-Temperature Fabrication and Performance of Polycrystalline CuI Films as Transparent p-Type Semiconductors, Phys. Status Solidi A. 216 (2019) 1700782. https://doi.org/10.1002/pssa.201700782.
[25] P. Storm, M.S. Bar, G. Benndorf, S. Selle, C. Yang, H. von Wenckstern, M. Grundmann, M. Lorenz, High mobility, highly transparent, smooth, p-type CuI thin films grown by pulsed laser deposition, APL Mater. 8 (2020) 091115. https://doi.org/10.1063/5.0021781.
[26] F. Geng, L. Yang, B. Dai, S. Guo, G. Gao, L. Xu, J. Han, A. Bolshakov, J. Zhu, Enhanced transmittance and mobility of p-type copper iodide thin films prepared at room temperature via a layer-by-layer approach, Surf. Coat. Technol. 361 (2019) 396–402. https://doi.org/10.1016/j.surfcoat.2019.01.057.
[27] A. Annadi, N. Zhang, D.B.K. Lim, H. Gong, Hole Transport Modulations in Low Dimensional γ-CuI Films: Implication for High Figure of Merit and Thin Film Transistors, ACS Appl. Electron. Mater. 1 (2019) 1029–1037. https://doi.org/10.1021/acsaelm.9b00177.
[28] Z. Zheng, A. Liu, S. Wang, B. Huang, K.W. Wong, X. Zhang, S.K. Hark, W.M. Lau, Growth of highly oriented (110) γ-CuI film with sharp exciton band, J. Mater. Chem. 18 (2008) 852. https://doi.org/10.1039/b719452h.
[29] M. Yashima, Q. Xu, A. Yoshiasa, S. Wada, Crystal structure, electron density and diffusion path of the fast-ion conductor copper iodide CuI, J. Mater. Chem. 16 (2006) 4393. https://doi.org/10.1039/b610127e.
[30] Y. Seguchi, T. Soejima, Facile vapor-phase synthesis of copper nanostructures on cuprous iodide films, Vacuum. 144 (2017) 53–62. https://doi.org/10.1016/j.vacuum.2017.07.017.
[31] M.R. Johan, K. Si-Wen, N. Hawari, N.A.K. Aznan, Synthesis and Characterization of Copper (I) Iodide Nanoparticles via Chemical Route, Int J Electrochem Sci. 7 (2012) 9.
[32] D.A. Keen, S. Hull, The high-temperature structural behaviour of copper(I) iodide, J. Phys. Condens. Matter. 7 (1995) 5793–5804. https://doi.org/10.1088/0953-8984/7/29/007.
[33] S. Hull, D.A. Keen, W. Hayes, N.J.G. Gardner, Superionic behaviour in copper (I) iodide at elevated pressures and temperatures, J. Phys. Condens. Matter. 10 (1998) 10941–10954. https://doi.org/10.1088/0953-8984/10/48/015.

[34] S. Hull, D.A. Keen, High-pressure polymorphism of the copper(I) halides: A neutron-diffraction study to ∼10 GPa, Phys. Rev. B. 50 (1994) 5868–5885. https://doi.org/10.1103/PhysRevB.50.5868.
[35] G. Lin, F. Zhao, Y. Zhao, D. Zhang, L. Yang, X. Xue, X. Wang, C. Qu, Q. Li, L. Zhang, Luminescence Properties and Mechanisms of CuI Thin Films Fabricated by Vapor Iodization of Copper Films, Materials. 9 (2016) 990. https://doi.org/10.3390/ma9120990.
[36] K. Zhao, G.O. Ngongang Ndjawa, L.K. Jagadamma, A.E. Labban, H. Hu, Q. Wang, R. Li, M. Abdelsamie, P.M. Beaujuge, A. Amassian, Highly efficient organic solar cells based on a robust room-temperature solution-processed copper iodide hole transporter, Nano Energy. 16 (2015) 458–469. https://doi.org/10.1016/j.nanoen.2015.07.018.
[37] C. Yang, E. Rose, W. Yu, T. Stralka, F. Geng, M. Lorenz, M. Grundmann, Controllable Growth of Copper Iodide for High-Mobility Thin Films and Self-Assembled Microcrystals, ACS Appl. Electron. Mater. 2 (2020) 3627–3632. https://doi.org/10.1021/acsaelm.0c00692.
[38] S.A. Mohamed, J. Gasiorowski, K. Hingerl, D.R.T. Zahn, M.C. Scharber, S.S.A. Obayya, M.K. El-Mansy, N.S. Sariciftci, D.A.M. Egbe, P. Stadler, CuI as versatile hole-selective contact for organic solar cell based on anthracene-containing PPE–PPV, Sol. Energy Mater. Sol. Cells. 143 (2015) 369–374. https://doi.org/10.1016/j.solmat.2015.07.003.
[39] C. Adamo, V. Barone, Toward reliable density functional methods without adjustable parameters: The PBE0 model, J. Chem. Phys. 110 (1999) 6158–6170. https://doi.org/10.1063/1.478522.
[40] D. Kim, M. Nakayama, O. Kojima, I. Tanaka, H. Ichida, T. Nakanishi, H. Nishimura, Thermal-strain-induced splitting of heavy- and light-hole exciton energies in CuI thin films grown by vacuum evaporation, Phys. Rev. B. 60 (1999) 13879–13884. https://doi.org/10.1103/PhysRevB.60.13879.
[41] Y. Wang, P. Miska, D. Pilloud, D. Horwat, F. Mücklich, J.F. Pierson, Transmittance enhancement and optical band gap widening of Cu_2O thin films after air annealing, J. Appl. Phys. 115 (2014) 073505. https://doi.org/10.1063/1.4865957.
[42] H. Sun, M. Arab Pour Yazdi, P. Briois, J.-F. Pierson, F. Sanchette, A. Billard, Towards delafossite structure of Cu–Cr–O thin films deposited by reactive magnetron sputtering: Influence of substrate temperature on optoelectronics properties, Vacuum. 114 (2015) 101–107. https://doi.org/10.1016/j.vacuum.2015.01.009.
[43] K.K. Chinnakutti, V. Panneerselvam, D. Govindarajan, A. kumar Soman, K. Parasuraman, S. Thankaraj Salammal, Optoelectronic and electrochemical behaviour of γ-CuI thin films prepared by solid iodination process, Prog. Nat. Sci. Mater. Int. 29 (2019) 533–540. https://doi.org/10.1016/j.pnsc.2019.09.005.
[44] M. Graužinytė, S. Botti, M.A.L. Marques, S. Goedecker, J.A. Flores-Livas, Computational acceleration of prospective dopant discovery in cuprous iodide, Phys. Chem. Chem. Phys. 21 (2019) 18839–18849. https://doi.org/10.1039/C9CP02711D.
[45] T. Leijtens, I.-K. Ding, T. Giovenzana, J.T. Bloking, M.D. McGehee, A. Sellinger, Hole Transport Materials with Low Glass Transition Temperatures and High Solubility for Application in Solid-State Dye-Sensitized Solar Cells, ACS Nano. 6 (2012) 1455–1462. https://doi.org/10.1021/nn204296b.
[46] P. Pattanasattayavong, N. Yaacobi-Gross, K. Zhao, G.O.N. Ndjawa, J. Li, F. Yan, B.C. O'Regan, A. Amassian, T.D. Anthopoulos, Hole-Transporting Transistors and Circuits Based on the Transparent Inorganic Semiconductor Copper(I) Thiocyanate (CuSCN) Processed from Solution at Room Temperature, Adv. Mater. 25 (2013) 1504–1509. https://doi.org/10.1002/adma.201202758.
[47] J.A. Christians, R.C.M. Fung, P.V. Kamat, An Inorganic Hole Conductor for Organo-Lead Halide Perovskite Solar Cells. Improved Hole Conductivity with Copper Iodide, J. Am. Chem. Soc. 136 (2014) 758–764. https://doi.org/10.1021/ja411014k.
[48] A.N. Gruzintsev, W.N. Zagorodnev, Effect of annealing on the luminescence of p-CuI crystals, Semiconductors. 46 (2012) 149–154. https://doi.org/10.1134/S1063782612020133.

[49] S. Koyasu, N. Umezawa, A. Yamaguchi, M. Miyauchi, Optical properties of single crystalline copper iodide with native defects: Experimental and density functional theoretical investigation, J. Appl. Phys. 125 (2019) 115101. https://doi.org/10.1063/1.5082865.
[50] T. Jun, T. Handa, K. Sim, S. Iimura, M. Sasase, J. Kim, Y. Kanemitsu, H. Hosono, One-step solution synthesis of white-light-emitting films via dimensionality control of the Cs–Cu–I system, APL Mater. 7 (2019) 111113. https://doi.org/10.1063/1.5127300.

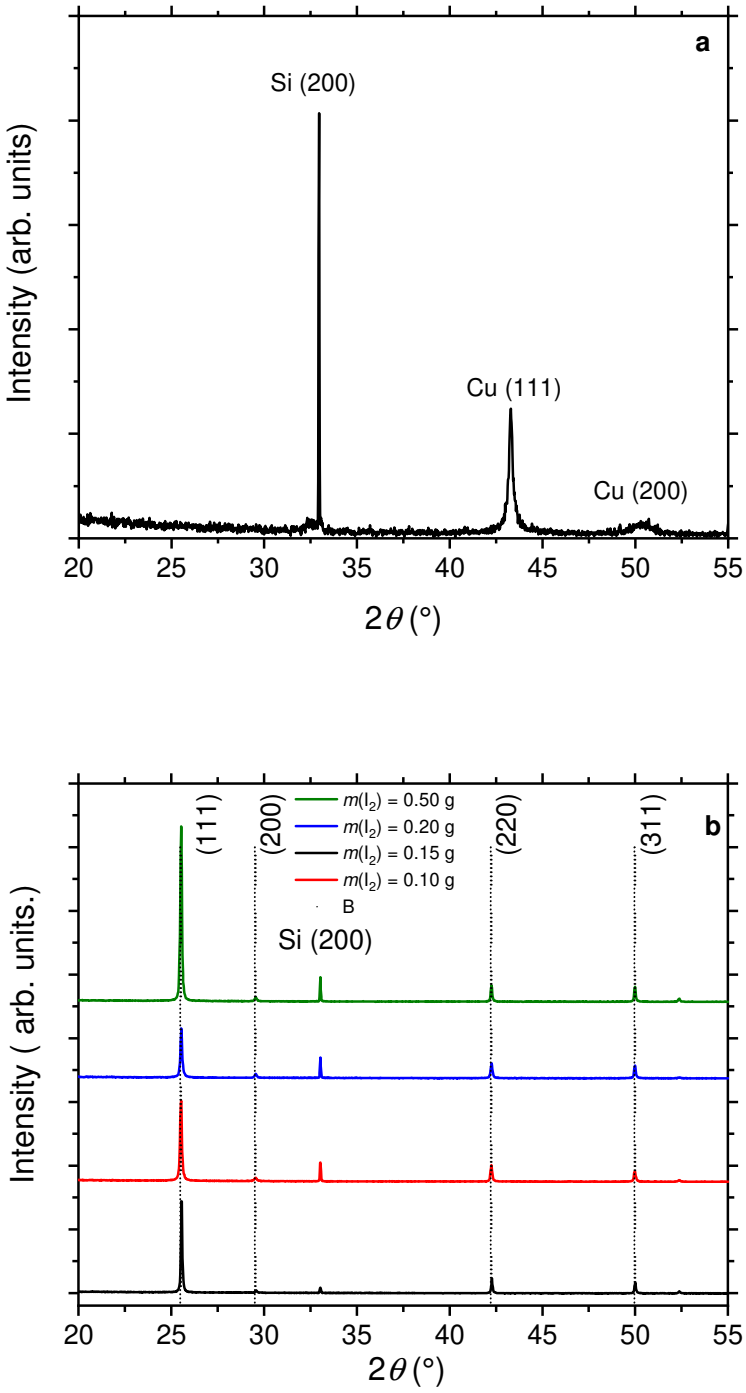

Figure 1: a) X-ray diffractogram of an as-deposited Cu film on Si substrate. b) Series of X -ray diffractograms of CuI films synthesized with different amounts of iodine. The vertical dashed lines correspond to the theoretical positions of γ-CuI diffraction peaks.

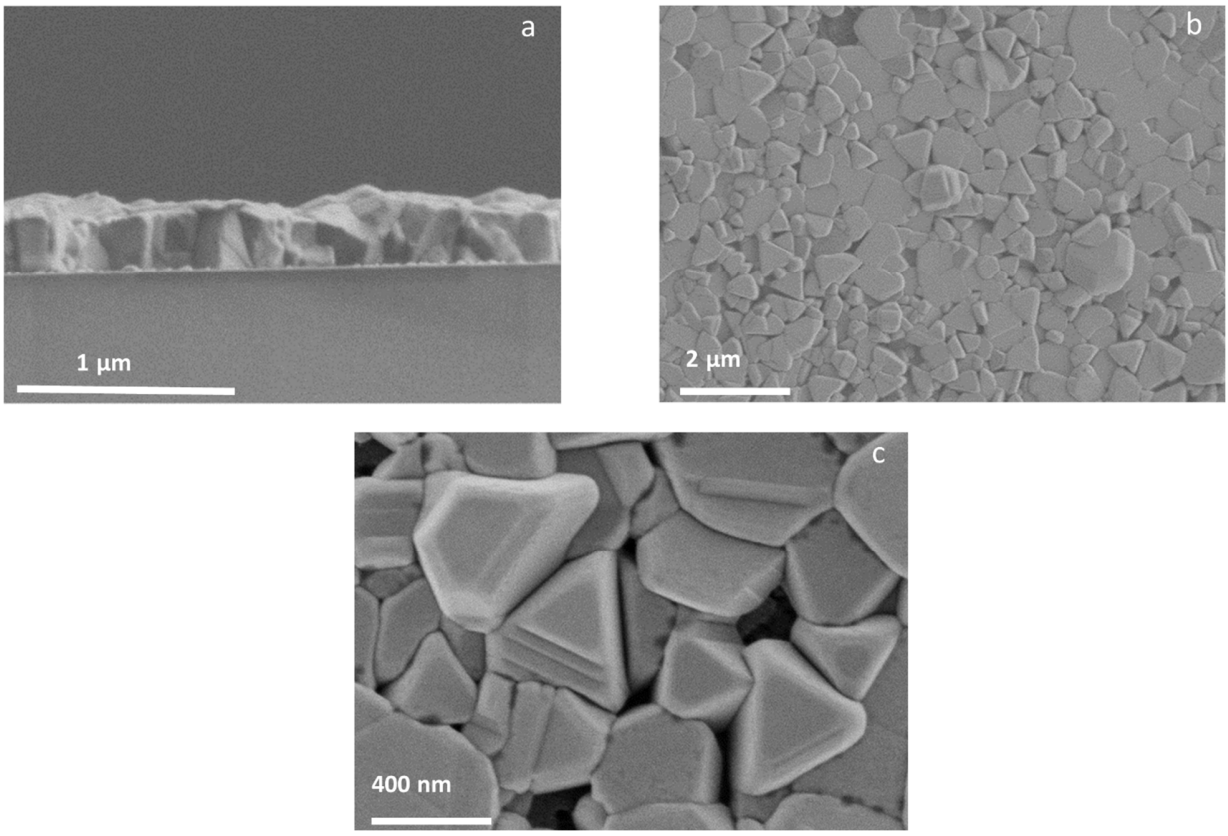

Figure 2: SEM cross section of a film prepared with 0.15 g I_2 deposited on silicon substrate a) SEM surface image of the same film b) and surface magnification of a film prepared on a glass substrate with the same amount of iodine c).

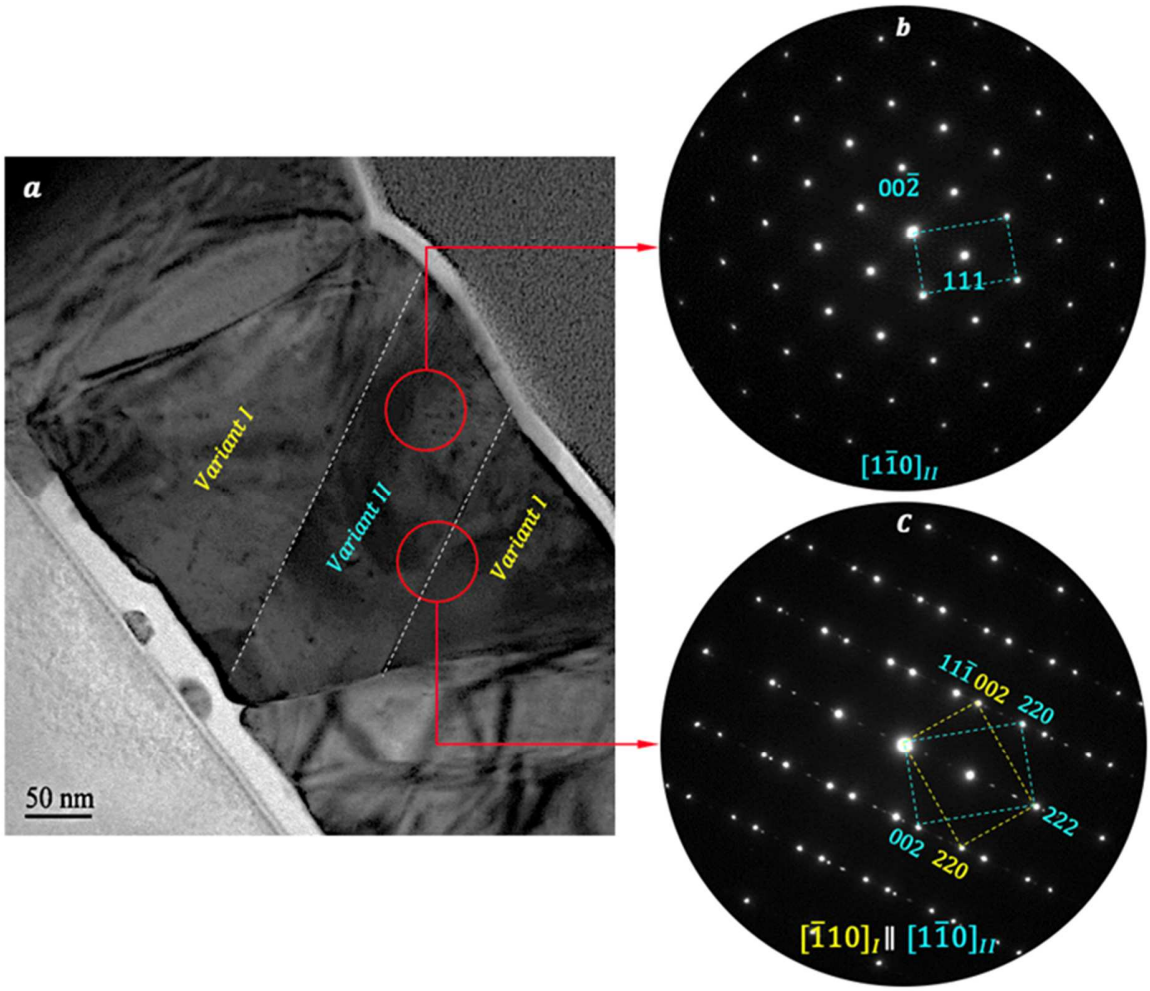

Figure 3: a) Bright field TEM micrograph showing twin related variants of thin CuI film (300 nm thick) deposited on silicon substrate. b) Corresponding electron diffraction pattern recorded along $[1\bar{1}0]_{II}$ zone axis. c) Composite electron diffraction pattern recorded along $[\bar{1}10]_I \parallel [1\bar{1}0]_{II}$ zone axes.

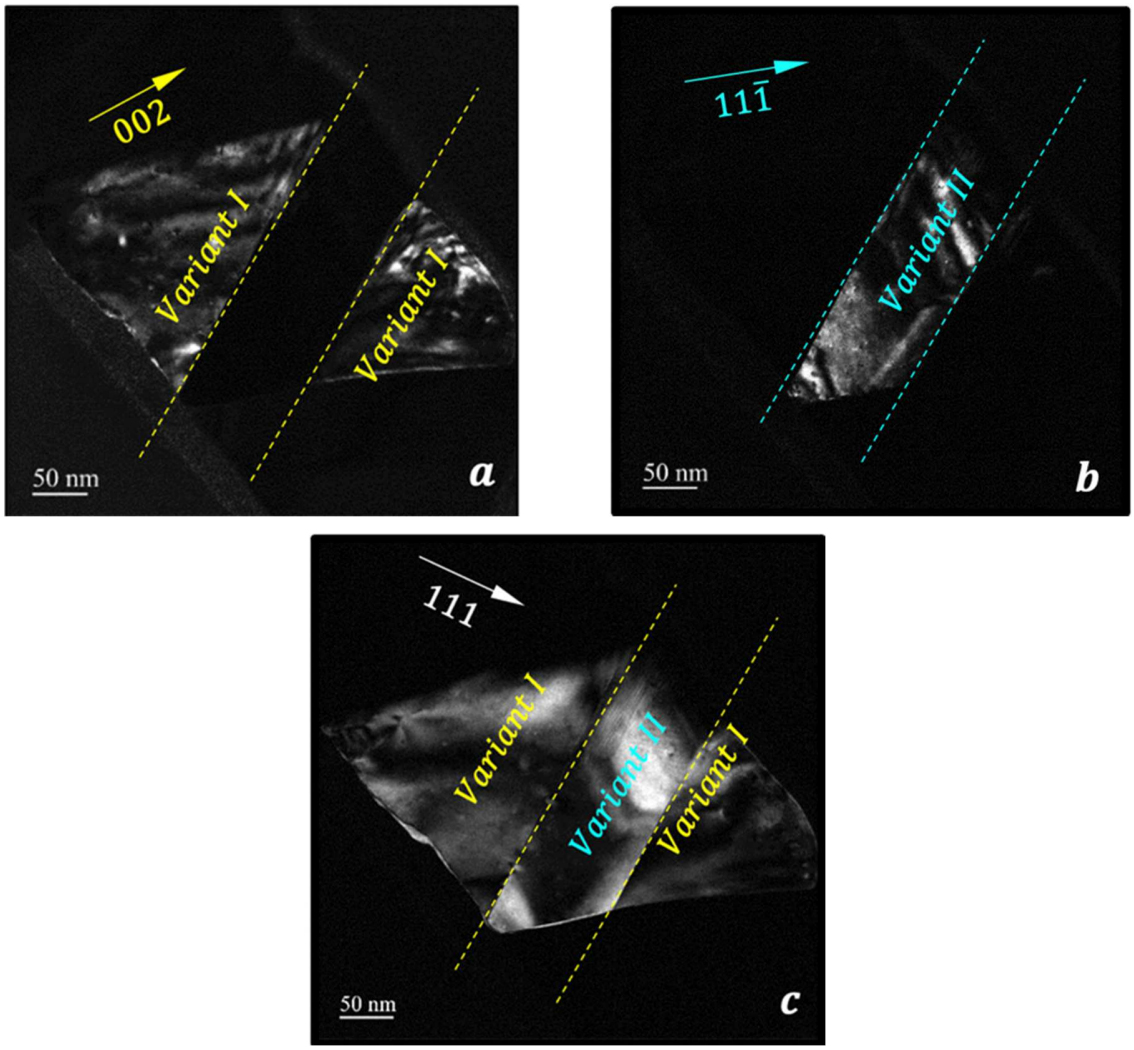

Figure 4: Series of dark field TEM images recorded with a) $\vec{g}_I = (002)$, b), $\vec{g}_{II} = (11\bar{1})$ and c) $\vec{g}_{I,II} = (11\bar{1})$, revealing two twin-related variants (I and II). One can notice that $(1\bar{1}1)$ is common to the two twin-related variants, is perpendicular to the twin plane.

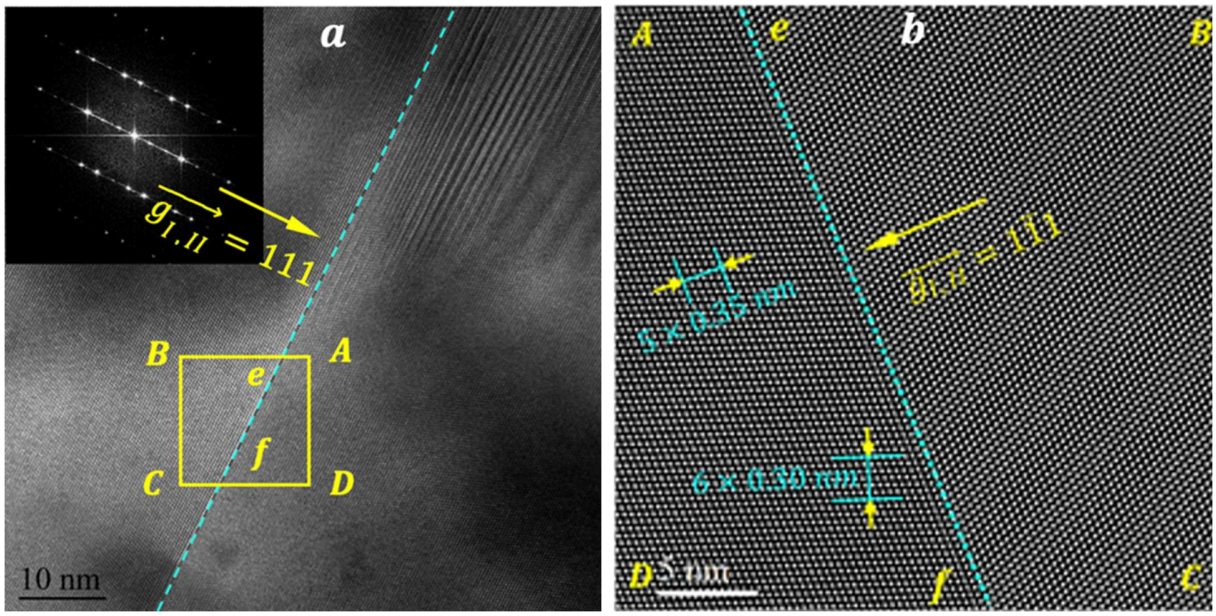

Figure 5: a) HRTEM micrograph recorded along [011] exhibiting two twin-related variants with, in the inset, the corresponding Fast Fourier Transform (FFT). b) STEM micrograph recorded along the same $[\bar{1}10]_I \parallel [1\bar{1}0]_{II}$ zone axis and same area of interest exhibiting the twin plane separating the two twin-related variants. One can notice in Figure 5a, in addition to the twin-plane, stacking faults in the variant at right.

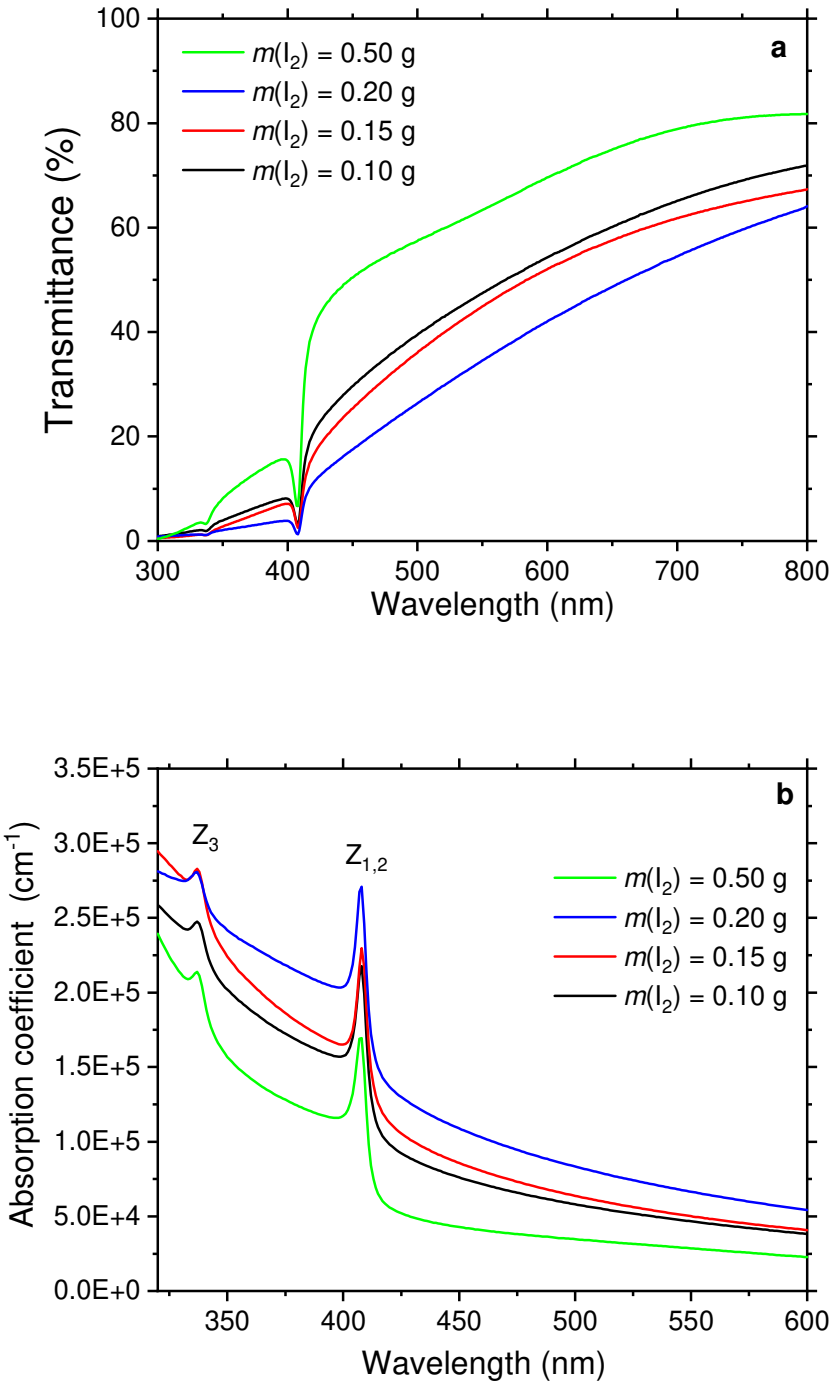

Figure 6: a) Transmission spectra of the CuI thin films synthesized with different amounts of iodine. b) Absorption coefficient evolution as a function of the wavelength.

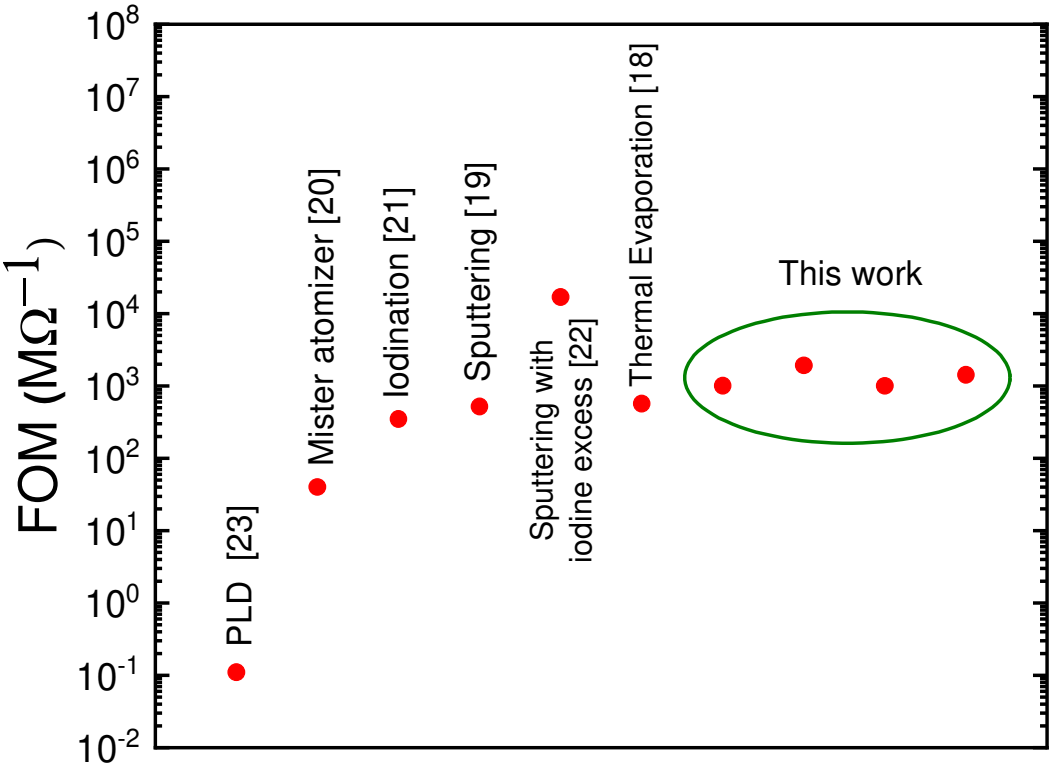

Figure 7: Evolution of the figure of merit of CuI films from the present work and from the literature.

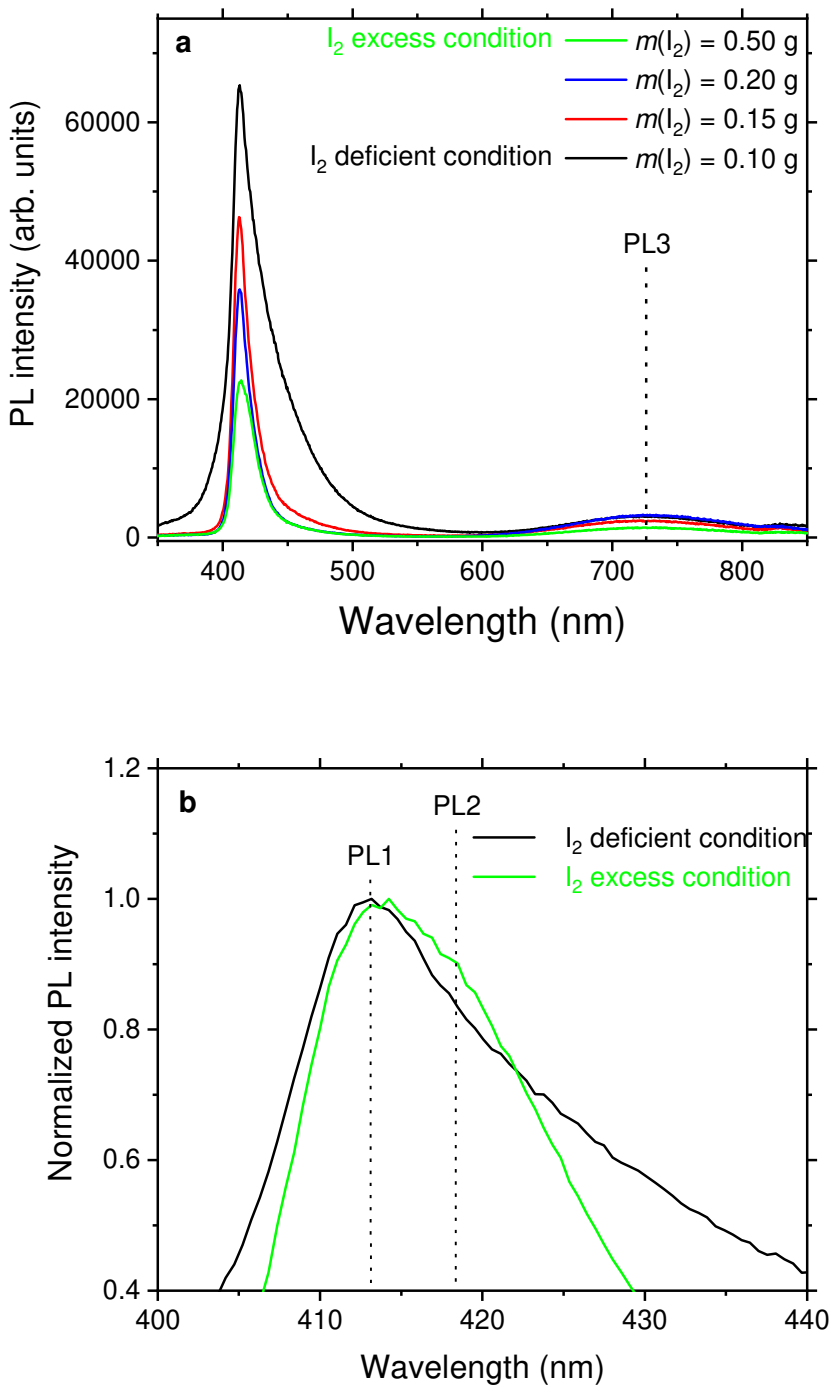

Figure 8: a) Photoluminescence spectra of the γ-CuI thin film with different amounts of iodine excited by 320 nm. b) magnification of the high energy peak to show the influence of the iodine amount on the shoulder at 418 nm.

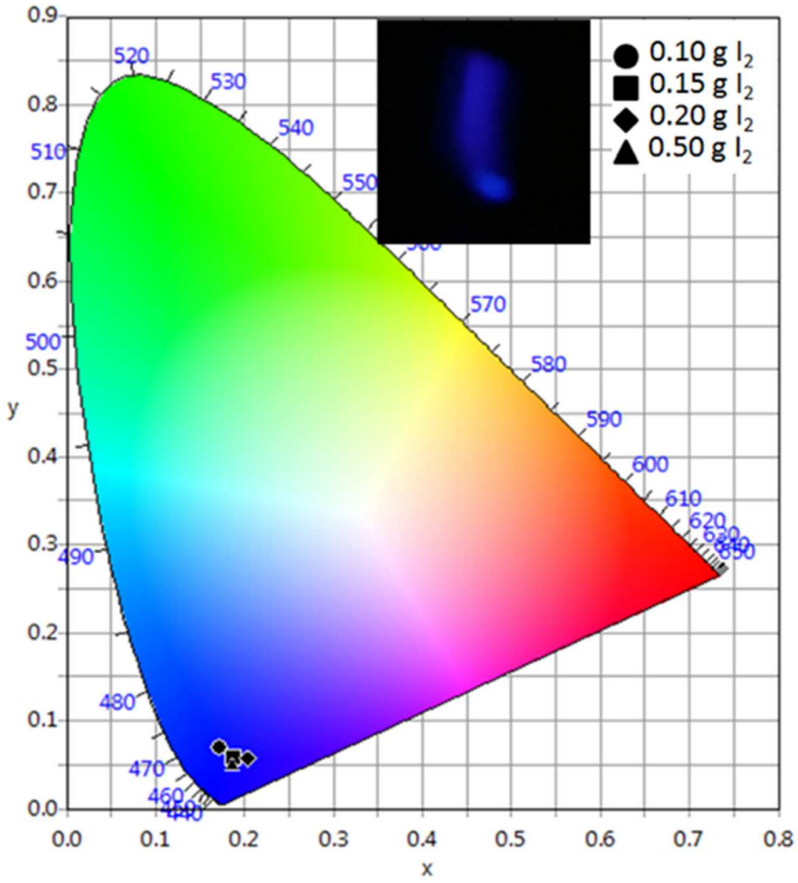

Figure 9: CIE chromaticity diagram coordinates of the four samples. The inset corresponds to a photo of the blue emission from one sample under UV-excitation

Table 1 Resistivity (ρ), b) mobility (μ) and c) hole density (p) of the γ-CuI thin film

I_2 mass (g)	Resistivity (Ω cm)	Conductivity (S cm^{-1})	Mobility (cm^2 V^{-1} s^{-1})	Carrier concentration (cm^{-3})
0.10	4.4×10^{-2}	22.7	49.6	3.1×10^{18}
0.15	2.1×10^{-2}	47.4	6.9	4.3×10^{19}
0.20	3.3×10^{-2}	30.8	35.5	5.7×10^{18}
0.50	5.1×10^{-2}	19.6	45.9	1.4×10^{18}

Table 2: The figure of merit of γ-CuI thin films prepared by various techniques and in the present work.

Preparation method	Thickness (nm)	*T* (%)	Conductivity (S cm^{-1})	FOM ($M\Omega^{-1}$)	Ref.
PLD	500	80	5×10^{-4}	0.11	[23]
Mister atomizer	550	75	0.21	40	[20]
Iodination	500	49	5	350	[21]
Sputtering	100	70	18.5	518	[19]
Sputtering with I_2 excess	200	72	283	17000	[22]
Thermal evaporation	120	77	13.9	570	[18]
Sputtering + iodination	300	51	22.7	1010	Present work
Sputtering + iodination	300	48	47.4	1920	Present work
Sputtering + iodination	300	40	30.8	1003	Present work
Sputtering + iodination	300	66	19.6	1425	Present work